Nanoscale Res Lett (2009) 4:503–512
DOI 10.1007/s11671-009-9273-2

NANO EXPRESS

Tapered ZnO Whiskers: {*hkil*}-Specific Mosaic Twinning VLS Growth from a Partially Molten Bottom Source

Bang-Hao Huang · Pouyan Shen · Shuei-Yuan Chen

Received: 14 December 2008 / Accepted: 6 February 2009 / Published online: 25 February 2009
© to the authors 2009

Abstract Zn particulates overlaid with wurtzite (W)-type ZnO condensates having nearly orthogonal $\{10\bar{1}1\}$ and $\{11\bar{2}1\}$ facets were found to self-catalyze unusual tapered W-ZnO whiskers upon isothermal atmospheric annealing, i.e., thermal oxidation, at 600 °C. Analytical electron microscopic observations indicated that such whiskers formed tapered slabs having mosaic $\{10\bar{1}1\}$ and $\{2\bar{1}\bar{1}1\}$ twinned domains. The tapered whiskers can be rationalized by an alternative vapor–liquid–solid growth, i.e., {*hkil*}-specific coalescence twinning growth from the ZnO condensates taking advantage of a partially molten bottom source of Zn and the adsorption of atoms at the whisker tips and ledges under the influence of capillarity effect. The tapered whiskers having strong photoluminescence at 391 nm and with a considerable flexibility could have potential applications.

Keywords ZnO · Whiskers · Pulsed laser ablation · VLS · Photoluminescence

Introduction

The motivation of this research was to prove experimentally that tapered whiskers bounded by specific crystal surfaces can be formed by an unusual vapor–liquid–solid (VLS) growth mechanism, i.e., {*hkil*}-specific coalescence twinning growth from crystalline condensates taking advantage of a partially molten bottom source rather than a small liquid globular at the tip of the whisker.

The VLS mechanism of single crystal growth [1] was generally accepted to be a liquid-mediated growth at the tip of an elongated crystal where mass transportation from vapor to solid via liquid occurs. In general, the intermediate liquid has nothing to do with the growth direction of the elongated crystal via this mechanism unless there is partial crystallinity of liquid that affects lattice match and hence the crystallographic relationship with the crystal underneath as experimentally proved for catalyst-free [2] or catalyst-guided [3] growth of wurtzite(W)-type ZnO nanowires/nanobelts having polar surfaces (0001) and $(0\bar{1}11)$ to minimize the electrostatic energy [4].

Recently, W-ZnO condensates prepared by pulsed laser ablation (PLA) in vacuum for nanosized and predominant surfaces $\{10\bar{1}1\}$ were used for self-catalyzed VLS growth of rod-like W-ZnO whiskers in air [5]. The resultant whiskers have characteristic globular tips yet unusual habit, i.e., extending along the zone axis of the well-developed polar surfaces $\{10\bar{1}1\}$ accompanied by $\{11\bar{2}1\}$-specific growth twinning and/or coalescence twinning for a beneficial fair coincidence-site lattice at the twin boundary [5]. Such W-ZnO whiskers with globular tips [5] are in accord with the commonly accepted VLS mechanism via liquid-mediated growth at the tip [1]. The observed twin boundary $\{11\bar{2}1\}$ [5] is additional to $(11\bar{2}2)$ [6–8], $(10\bar{1}1)$ [7], $(0\bar{1}14)$ [9], and $(01\bar{1}3)$ [10] reported for W-ZnO.

In this study, we report further the development of tapered whiskers from Zn particulates overlaid with twinned W-ZnO condensates acting as seeds for VLS growth via a thermal oxidation process. There is significant difference in this study in respect of our previous experiments

B.-H. Huang · P. Shen
Department of Materials and Optoelectronic Science, Institute of Materials Science and Engineering, National Sun Yat-sen University, Kaohsiung, Taiwan, ROC

S.-Y. Chen (✉)
Department of Mechanical and Automation Engineering, I-Shou University, Kaohsiung, Taiwan, ROC
e-mail: steven@isu.edu.tw

i.e., the usage of an oxygen environment instead of the residual oxygen-containing vacuum [5] to form Zn particulates overlaid with W-ZnO nanocrystallites during PLA. (Zn particulates as the solidification products of molten plumes were significantly formed via PLA in air rather than in vacuum, because the former process has a significant air-breaking effect to broaden the beam and hence to produce more molten Zn particulates covered with ZnO condensates in order to prevent from complete oxidation.) Such Zn particulates overlaid with W-ZnO nanocrystallites are essential to the present formation of tapered W-ZnO whiskers via a thermal oxidation VLS process from a partially molten bottom source of Zn upon annealing, in drastic contrast with our previously studied case of VLS growth at a partially molten globular tip [5].

Thermal oxidization of Zn is popular for synthesizing nanoneedles or nanobelts of ZnO. The effect of H_2O_2 pre-oxidation of Zn [11] and the co-existence of Au nanoparticles with Zn at temperatures [12] on the fabrication of W-ZnO nanoneedles or nanobelts has been studied. Direct oxidation of zinc foil in alkaline zincate ion solution at near room temperature [13] and a simple hydrothermal synthesis [14] were also found to cause the formation of highly [0001]-oriented ZnO nanoneedle/nanorods arrays. There are other growth manners through solution chemistry, such as an electrochemical deposition process to control the growth of ZnO taper-tubes [15]; an in situ template route to fabricate ZnO taper-tubes through chemical etching reaction [16]; and an in situ chemistry strategy to convert ZnO nanorods into ZnO/ZnS nanocable arrays [17].

We emphasize here that a partially molten bottom source of Zn overlaid with W-ZnO condensates having nearly orthogonal $\{10\bar{1}1\}$ and $\{11\bar{2}1\}$ facets accounts for $\{hkil\}$-specific coalescence and hence VLS growth of the tapered whiskers extending along mosaic twin domain boundaries rather than commonly observed [0001] direction. This study sheds light on an alternative VLS growth mechanism for other compound whiskers to be explored in the future.

Experimental

Zn target with negligible impurities (99.9% pure) was subjected to energetic Nd-YAG-laser (Lotis, 1064 nm in wavelength, beam mode: TEM00) under oxygen flow rate of 50 L/min in air, rather than vacuum as in our previous experiments [5], so that abundant Zn particulates covered with W-ZnO nanocondensates can be produced. These particulates with round surface and irregular shape (Appendix) act as a partially molten bottom source of Zn for the present thermal oxidation VLS growth upon annealing as mentioned. (Particulates were commonly accepted to be solidified from molten plumes during a PLA process [18].) The nearly pure oxygen gas was introduced into an open air chamber at the specified flow rate under room temperature and pressure conditions, i.e., near 25 °C and 1 atm.

Pulse energy of 560 mJ/pulse, i.e., power density of 1.17×10^{12} W/cm^2 given pulse time duration of 16 ns at 10 Hz (Q-switch) on focused area of 0.03 mm^2 was employed in the present PLA process. (A peak power density as high as 1.17×10^{11} W/cm^2 rather than a mean power density is of concern to the rapid heating–cooling, and hence to the phase and size selection of the condensates in the present PLA process.) Soda-lime glass or Zn plate at a distance of 25–10 mm from the target was used as a substrate to collect the condensates and particulates during PLA for a total of 10 min. The angle of incidence of the laser beam was maintained at ca. 20 degree in order to scan over a part of the moving target and to assure a satisfactory yield of deposit on the substrate in parallel to the target. The deposits with a common yield of 0.2-μm thickness per minute on the two different substrates were then annealed at 600 °C in air for a specified time up to 1 h (Appendix) in order to study the substrate effect, if any, on the formation of the tapered W-ZnO whiskers having an approximate 10% volume ratio of whiskers with respect to the partially molten particulates of bulk Zn with a melting point at 420 °C [19].

X-ray diffraction (XRD, CuKα, D5000 instrument) was used to study the orientation change, if any, of the W-ZnO and Zn deposits on glass upon annealing. High resolution XRD (CuKα, D1 instrument) step-scan with 0.001 degree increment of 2θ was also employed to resolve the nearly superimposed $\{10\bar{1}1\}_{W-ZnO}$ and $(0002)_{Zn}$ peaks. Scanning electron microscopy (SEM, JEOL 6330, 10 kV) was used to characterize the microstructure changes, in particular the whisker development, due to post-deposition annealing. The W-ZnO whiskers retrieved from the glass substrate were dispersed in alcohol and dipped onto copper grids overlaid with a carbon-coated collodion film for field emission transmission electron microscopy (TEM, FEI Tecnai G2 F20 at 200 kV) study coupled with selected area electron diffraction (SAED), and point-count energy dispersive X-ray (EDX) analysis at a beam size of 5 nm. The EDX analysis was performed using K shell counts for Zn and O, and the principle of ratio method without absorption correction [20].

The PL measurements were carried out at room temperature by Micro photoluminescence (PL) spectroscopy (Jobin Yvon T64000 Micro-PL/Raman Spectroscopy). The excitation source was the 325-nm line of a He–Cd laser. More than five independent PL runs were conducted for the tapered W-ZnO whiskers in order to compare with the PL result of a polycrystalline W-ZnO standard prepared by sintering at 1400 °C for 3 h in air.

Results and Discussion

Results of PLA Process

The XRD whole trace showed a strong preferred orientation of $(0001)_{Zn}$ and $\{10\bar{1}1\}_{W-ZnO}$ as deposited on glass (Fig. 1). The corresponding high resolution XRD step-scan showed the resolved $(10\bar{1}1)_{W-ZnO}$ and $(0002)_{Zn}$ peaks. Such preferred orientations are the same as the condensates overlaid on glass by PLA in vacuum [5] and can be rationalized by the shape-dependent orientation of the condensates on a noncrystalline substrate rather than a true epitaxy relationship with respect to a crystalline substrate. Optical polarized microscopic observations of the as-formed deposits on glass showed irregularly shaped Zn plumes and micron-sized Zn particulates in a matrix of W-ZnO nanocondensates (Fig. 2a). (It should be noted that PLA of Zn in a permanently oxygen-enriched environment did not cause uniform oxidized W-ZnO deposit. Instead, Zn particulates covered with W-ZnO nanocondensates were formed. This is due to rapid solidification of the particulates from a molten state and a concurrent condensation process for significant coverage of W-ZnO nanocondensates in a permanently oxygen-enriched PLA environment.)

Results of Annealing

After annealing, the preferred orientations of $(0001)_{Zn}$ and $(10\bar{1}1)_{W-ZnO}$ on glass became obscure and the nearly overlapped $\{10\bar{1}1\}_{W-ZnO}$ and $(0002)_{Zn}$ were hardly resolvable due to low diffraction intensities (Fig. 1b). Optical polarized microscopy indicated that the opaque Zn particulates were significantly coarsened having a blurred outline due to birefringent W-ZnO whiskers radiating from them (Fig. 2b).

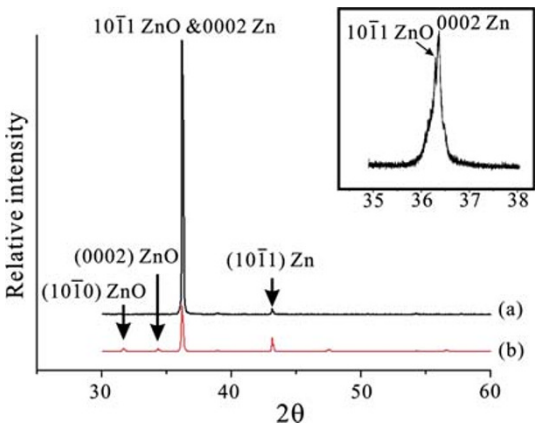

Fig. 1 X-ray diffraction (CuKα) traces of the Zn/W-ZnO deposits on glass: **a** as prepared by PLA; **b** further annealed at 600 °C. High-resolution XRD (CuKα) step-scan (inset) is able to resolve nearly overlapped $\{10\bar{1}1\}_{W-ZnO}$ and $(0002)_{Zn}$ for **a**, but not **b** because of low diffraction intensities

The same annealing condition did not cause the development of W-ZnO whiskers from a partially molten Zn plate (Fig. 2c), unless it has been deposited with Zn particulates overlaid with W-ZnO nanocondensates (Fig. 2d). (The Zn plate partly survived annealing at 600 °C despite a lower melting point of bulk Zn at 420 °C [19] and an unavoidable sublimation process with an activation energy of 197 KJmol^{-1} in the temperature range of 573–1073 K [21]. This can be explained by the presence of a passive oxide film on the bulk Zn plate upon annealing in air.) We conclude therefore that the deposit of Zn particulates overlaid with W-ZnO nanocondensates via the present PLA process are essential to the tapered whisker growth regardless of the substrate being glass or Zn plate.

The SEM images of the representative deposit on glass showed that the W-ZnO nanocondensates were coalesced as nano chain aggregate (NCA) or in a more closely packed manner on the surface of globular Zn particulates which also tended to coalesce (Fig. 3a). After annealing, tapered W-ZnO whiskers radiating from the coalesced Zn particulates appeared (Fig. 3b). According to point-count EDX analyses, the Zn particulate overlaid with tiny ZnO condensates (Fig. 3c) has more Zn counts than the W-ZnO whisker (Fig. 3d), both being immune from impurities.

Microstructures of Tapered Whiskers

The assembly of the tapered W-ZnO whiskers was observed by TEM bright field image (BFI) (Fig. 4a). The individual whisker (Fig. 4b) is twinned as indicated by SAED patterns taken from the root area (Fig. 4c) and nearby (Fig. 4d), which are slightly off and in exact $[2\bar{1}\bar{1}3]$ zone axis, respectively indexed according to a hexagonal W-type structure (space group $P6_3mc$) with lattice parameters a = 0.3249 nm and c = 0.5206 nm (JCPDS file 36–1451). It should be noted that such tapered whisker has well-developed $(2\bar{1}\bar{1}1)$ surface/steps to rest upon and hence in a preferred orientation close to $[2\bar{1}\bar{1}3]$ zone axis. The magnified areas near the tip (Fig. 4e and f) were also twinned with growth steps/ledges parallel to $\{1\bar{1}0\bar{1}\}$, although a curved surface possibly due to surface premelting as will be discussed later also occurred (Fig. 4e). By contrast, the tip (Fig. 4g) is a single crystal with $\{1\bar{1}0\bar{1}\}$ facets as indicated by lattice image and the 2-D forward Fourier transform. The $(11\bar{2}\bar{1})$ ledge, which is nearly orthogonal to the side surface $\{1\bar{1}0\bar{1}\}$ and an almost horizontal $(11\bar{2}\bar{1})$ plane in the $[2\bar{1}\bar{1}3]$ zone axis, also occurred near the tip.

As for the twinning scheme of the tapered W-ZnO whiskers, Fig. 5 shows well-developed twin plane $(2\bar{1}\bar{1}1)$ close to a top view in $[2\bar{1}\bar{1}3]$ zone axis. The lattice image (Fig. 5b) and the 2-D forward Fourier transform (Fig. 5c) showed lamellae fringes due to superimposition of the

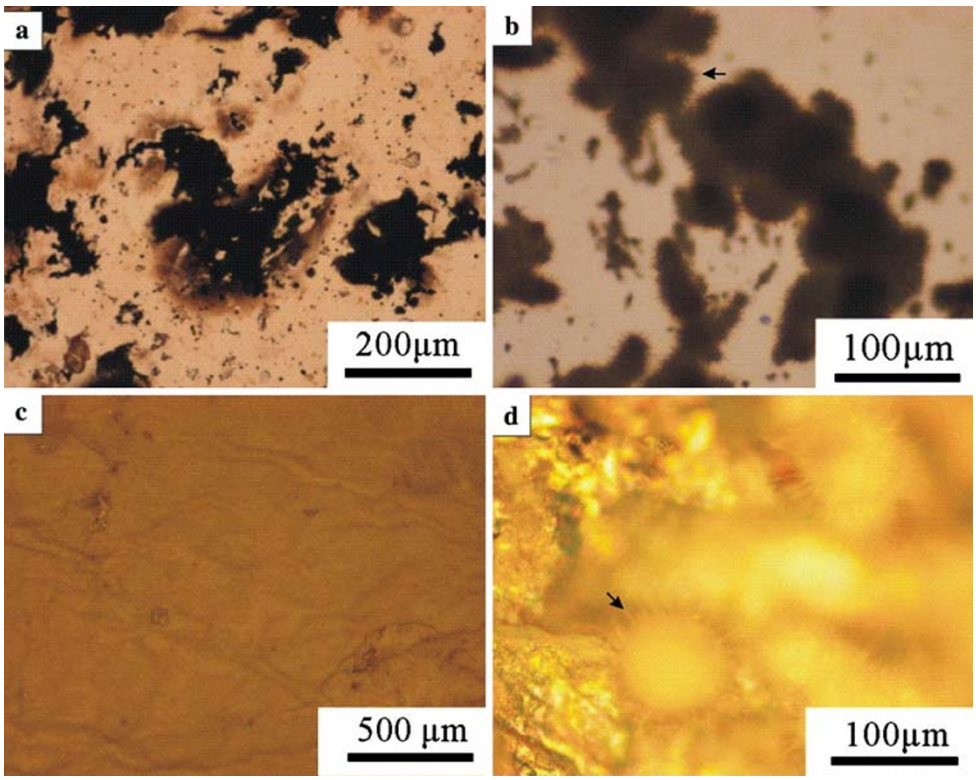

Fig. 2 Optical micrographs of Zn/W-ZnO samples via PLA deposition and/or annealing: **a** as-deposited on glass showing irregular-shaped Zn plumes and micron-sized Zn particulates (opaque) overlaid with hardly resolved W-ZnO nanocondensates (cf. SEM image in Fig. 3a); **b** further annealed sample showing significantly coarsened Zn particulates with blurred outline due to tapered W-ZnO whiskers (arrow) radiating from them (cf. SEM image in Fig. 3b); **c** blank Zn plate annealed without forming W-ZnO whiskers; **d** Zn plate with Zn/W-ZnO deposit via PLA and further annealed, showing W-ZnO whiskers (arrow) were developed from Zn particulates overlaid with W-ZnO condensates. Note: **a** and **b** were taken under transmission plane polarized light, whereas **c** and **d** under reflective light

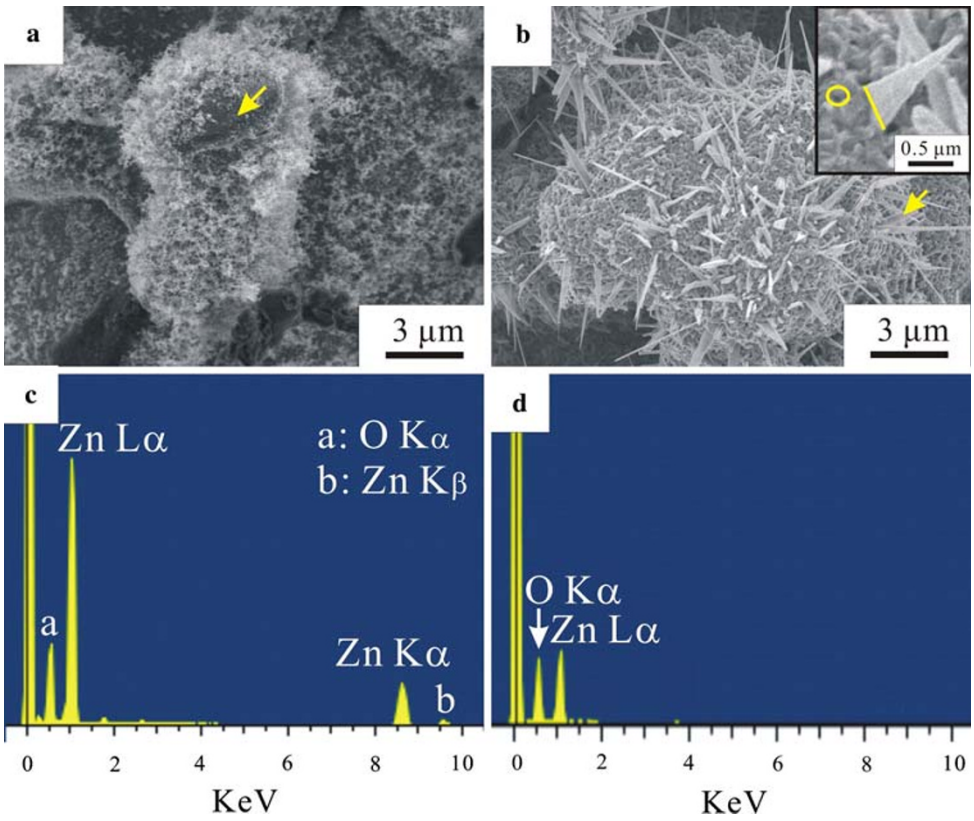

Fig. 3 SEM secondary electron images of Zn/W-ZnO particulates: **a** as-deposited by PLA, having W-ZnO condensates coalesced as NCA or in a closely packed manner on the surface of globular Zn particulates also in coalescence; **b** further annealed at 600 °C for 30 min to form tapered W-ZnO whiskers radiating from the coalesced particulates. The magnified image from the arrowed area (inset) shows a wide whisker base (underline) and smaller pores (circle) nearby (cf. text); **c** and **d** Point-count EDX spectra from the arrowed areas in **a** and **b**, respectively, showing more Zn counts from the Zn particulate overlaid with tiny ZnO condensates than the W-ZnO whiskers

bicrystals twinning over a horizontal $(2\bar{1}\bar{1}1)$ twin plane. The inverse Fourier transform and atomic simulation (Fig. 5d) further indicated that the $(2\bar{1}\bar{1}1)$ twin is about superimposition of the $(2\bar{1}\bar{1}1)$ plane by 52.2 degree off in order to show the lamellae fringes parallel to $(1\bar{1}0\bar{1})$ plane and the twinning spots as simulated in Fig. 5e.

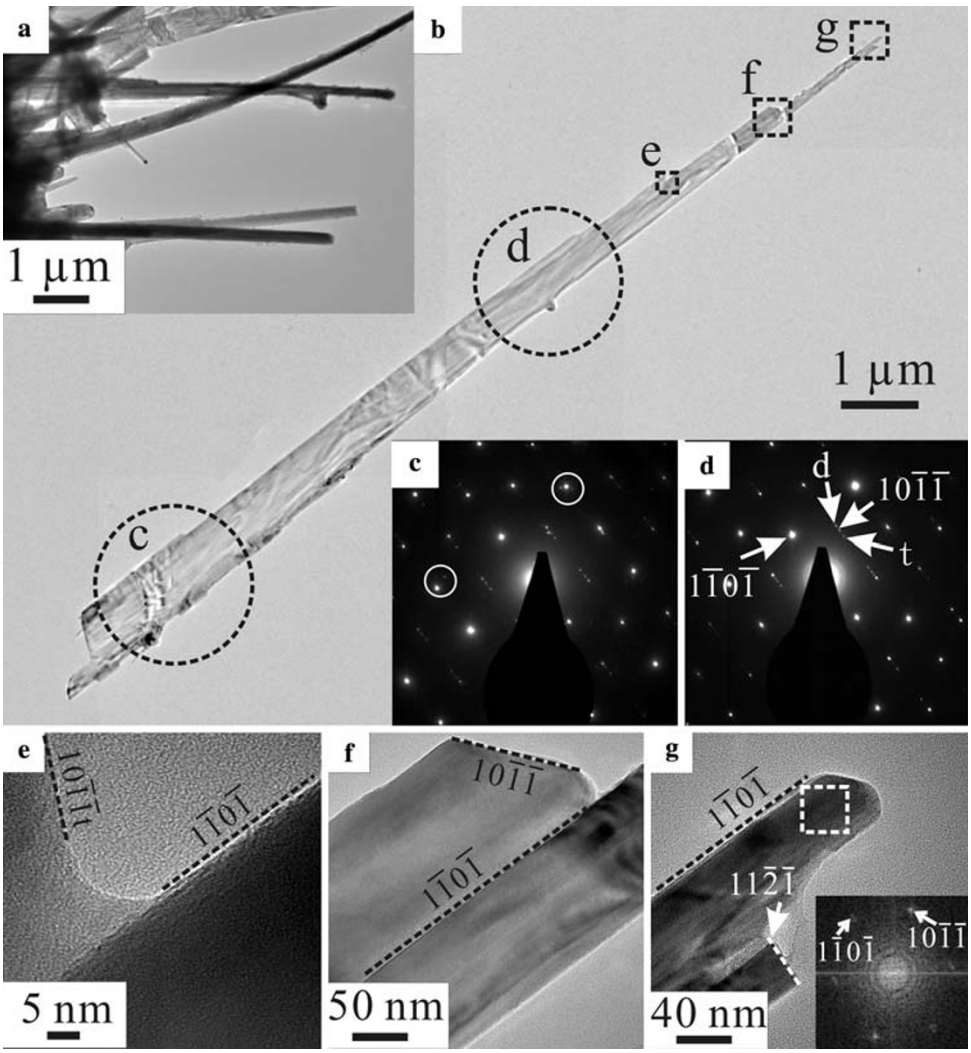

Fig. 4 TEM: **a** BFI of tapered W-ZnO whiskers; **b** Magnified BFI of an individual twinned whisker with SAED patterns; **c** and **d** taken from root and middle areas, respectively, showing the twin domains are slightly off $[2\bar{1}\bar{1}3]$ as indicated by spot splitting (circled) in **c**, but are in exact $[2\bar{1}\bar{1}3]$ zone axis in **d**, having twin spot denoted as t and double diffraction denoted as **d**; **e** and **f** Magnified BFIs from specified areas showing $\{1\bar{1}0\bar{1}\}$ facets and a curved growth ledge; **g** The Lattice image and the 2-D forward Fourier transform from the square region showing that the whisker tip is a single crystal with $\{1\bar{1}0\bar{1}\}$ facets as in the case of **e** and (**f**). Note: a nearby $(11\bar{2}\bar{1})$ ledge (arrowed) orthogonal to the side surface $\{1\bar{1}0\bar{1}\}$; The same specimen as in Fig. 3b

The tapered whisker has another twin plane, i.e., $(1\bar{1}0\bar{1})$, which is nearly orthogonal to $(2\bar{1}\bar{1}1)$ in local area to show a mosaic pattern. The BFI taken near the tip of such twinned ZnO whisker (Fig. 6a) shows vertical $(1\bar{1}0\bar{1})$ twin plane besides the nearly horizontal $(2\bar{1}\bar{1}1)$ twin plane in $[2\bar{1}\bar{1}3]$ zone axis. Lattice images and 2-D Fourier transform showed that the nearly horizontal $(2\bar{1}\bar{1}1)$ twin plane prevailed in area b in order to show twin and double diffraction spots (Fig. 6b). The $(1\bar{1}0\bar{1})$ twinning, however, prevailed edge on in local area I in Fig. 6c to show twin diffraction spots yet no significant double diffractions. The inverse 2-D Fourier transform of such an area and inserted atomic simulation further showed that the $(1\bar{1}0\bar{1})$ twin boundary is in fact a tilt boundary by 52° rotation about the $[2\bar{1}\bar{1}3]$ zone axis. By contrast, the area II in Fig. 6c is nearly a single crystal and hence free of twin diffraction spots. The point-count EDX analyses along the axial growth direction (not shown) indicated that the W-ZnO whisker is nearly stoichiometric in chemical composition except at steps/ledges and tips where a liquid-like layer, possibly due to surface premelting and EDX detection angle could cause apparent composition difference.

Scenario of Tapered Whisker Growth from a Partially Molten Bottom Source

The W-ZnO condensates on glass [5] or Zn plate (this study) were able to self-catalyze rod-like W-ZnO whiskers with characteristic globular tips, in accordance with the commonly accepted VLS mechanism via liquid mediated growth at the tip [1]. By contrast, the formation of the present tapered W-ZnO whiskers in this study involved an alternative VLS growth process from Zn particulates covered with nanocrystalline W-ZnO deposit on glass or Zn plate. It should be noted that tiny globular tip on top of twinned W-ZnO condensate typically causes a rod-like whisker with a well-developed $\{10\bar{1}1\}$ surface and $\{2\bar{1}\bar{1}1\}$-specific growth twinning or coalescence twinning by VLS growth [5]. On the other hand, much larger-sized Zn particulates, preferable via the PLA process in air (this

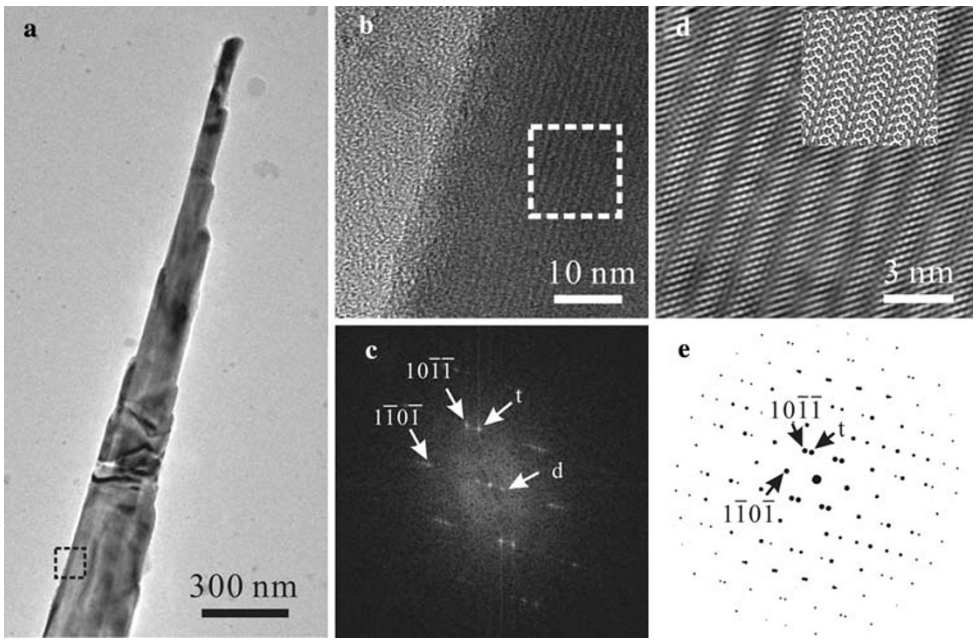

Fig. 5 TEM: **a** BFI of a tapered ZnO whisker with ledges and twinning; **b** Lattice image from the square region in **a** coupled with **c** forward- and **d** inverse Fourier transform from the square region in **b**, showing lamellae fringes due to superimposition of the bicrystals twinned over a nearly horizontal $(2\bar{1}\bar{1}1)$ twin plane in $[2\bar{1}\bar{1}3]$ zone axis. The inserted atomic simulation of two $(2\bar{1}\bar{1}1)$ slabs 2 nm in thickness superimposed by 52.2 degree off in **d** indeed shows lamellae-like $(1\bar{1}0\bar{1})$ fringes with corresponding twin spots (denoted as t) in the simulated diffraction pattern in **e**. The same specimen as in Fig. 3b

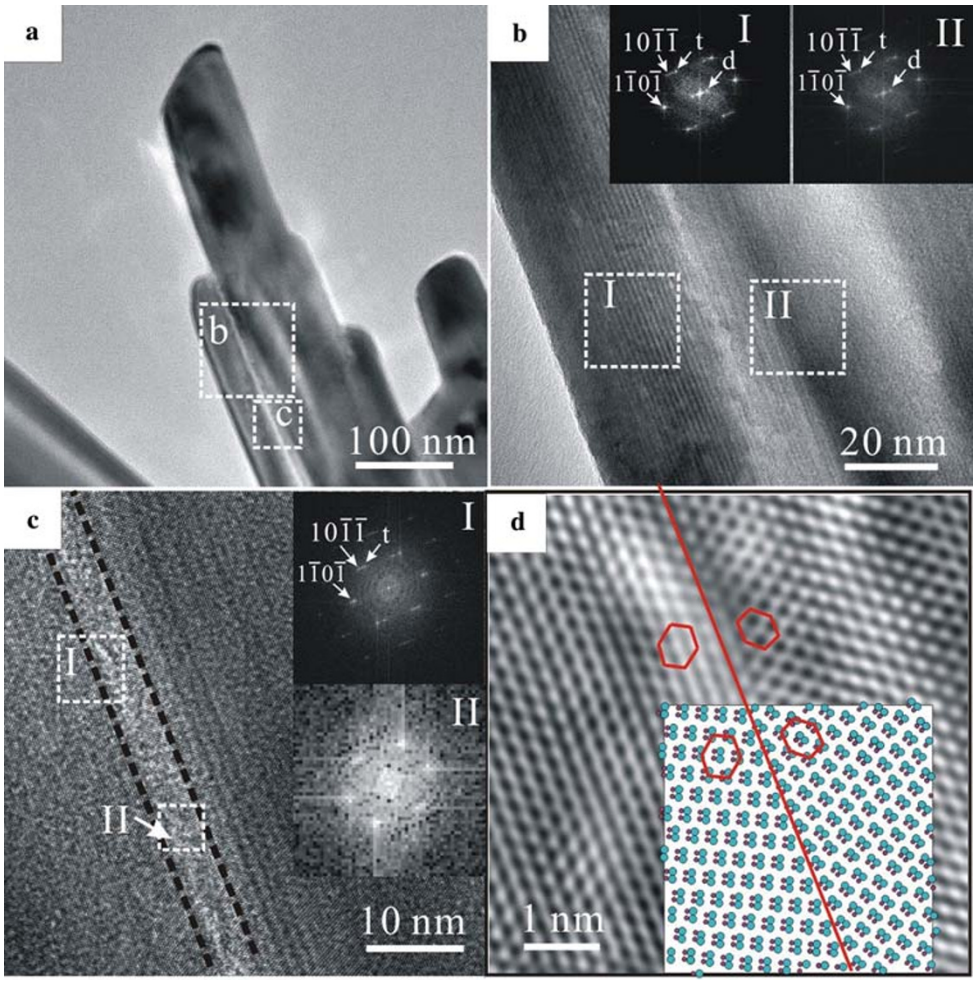

Fig. 6 TEM: **a** BFI taken near the tip of a tapered W-ZnO whisker with a $(1\bar{1}0\bar{1})$ twin plane edge on besides the $(2\bar{1}\bar{1}1)$ twin plane nearly horizontal in $[2\bar{1}\bar{1}3]$ zone axis; **b** and **c** Lattice images from the specified areas in **a** with Fourier transform from the square regions (I and II) inset. The nearly horizontal $(2\bar{1}\bar{1}1)$ twin plane prevails in region b, whereas an additional $(1\bar{1}0\bar{1})$ twin plane shows up edge on in area c as indicated by **d** inverse Fourier transform of the area I in **c** with inserted atomic simulation showing orientation difference of the basic units (outlined) across such a twin boundary. The same sample as in Fig. 3b

study) rather than vacuum [5] as mentioned, would act as a bottom reservoir for a thermal oxidation VLS process. Under such a case, there are a number of twinned W-ZnO condensates on top of a Zn particulate to impinge and coalesce mutually as a tapered whisker with unique $\{10\bar{1}1\}/\{2\bar{1}\bar{1}1\}$ mosaic twinning and growth ledges as depicted sequentially in Fig. 7. First, the W-ZnO seeds on Zn particulates underwent $\{10\bar{1}1\}$- and/or $\{2\bar{1}\bar{1}1\}$-specific coalescence twinning during laser ablation condensation (Fig. 7a). The W-ZnO whiskers with well-developed $\{10\bar{1}1\}$ and $\{2\bar{1}\bar{1}1\}$ surfaces and twin boundaries then developed anisotropically from such twinned seeds on the partially molten Zn particulates upon annealing (Fig. 7b). Such whiskers were impinged and assembled as tapered bundles with intimate intergrowth of such twinned domains, which are nearly orthogonal and hence a mosaic pattern (Fig. 7c). (Note that some $\{10\bar{1}1\}$ and $\{2\bar{1}\bar{1}1\}$ surfaces intersect at ca. 82 degree depending on the c/a ratio [5], see Appendix 1) The outward Zn and inward oxygen diffusion would occur across the ZnO/Zn interface and along specific surfaces and twin planes of the tapered bundles. The adsorption of atoms for a fair accommodation at the whisker tips and ledges would also proceed continuously under the influence of capillarity effect (Fig. 7d). In other words, we propose a sort of capillary diffusion of Zn atoms from the bottom to the tip of the whisker along the twinning edges and stepwise ledges as the source of tip growth to form a tapered whisker. Nucleation site saturation and later coalescence of the neighboring W-ZnO whiskers, in order to form a single crystal or twin, would occur predominantly in the early stage of this VLS growth process in order to have nearly the same size and aspect ratio of the tapered whiskers.

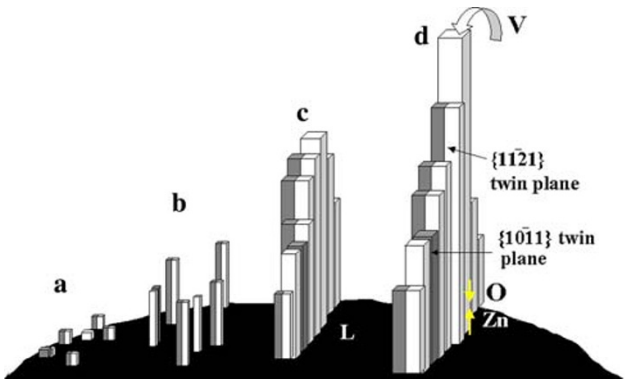

Fig. 7 Schematic drawing of the VLS growth of tapered ZnO whiskers from a partially molten bottom source of Zn in sequential stages: **a** $\{10\bar{1}1\}$ and/or $\{2\bar{1}\bar{1}1\}$ specific coalescence twinning (gray vs white domains) of the W-ZnO condensate seeds; **b** anisotropic growth of individual W-ZnO whisker with well-developed $\{10\bar{1}1\}$ and $\{2\bar{1}\bar{1}1\}$ surfaces and twin boundaries; **c** impingement and assembling to form tapered bundles with intimate intergrowth of $\{10\bar{1}1\}$- and $\{2\bar{1}\bar{1}1\}$-twinned domains in a mosaic pattern; **d** outward Zn and inward oxygen diffusion via $\{10\bar{1}1\}/\{2\bar{1}\bar{1}1\}$ surfaces and twin boundaries in accompaniment with adsorption of vapor atoms at the whisker tip and ledges under the influence of capillarity effect

It should be noted that the Zn liquid splashed out of a compact oxide film shell could oxidize and grow as W-ZnO nanoneedles in a thermal oxidation process [22]. Under such a case, the needles grow out from the extremities and corners of the Zn nanoparticles [22]. By contrast, the tapered W-ZnO whiskers in this study were hardly derived from the splashed liquid because the tapered whiskers have a much wider base than the pores on the partially molten particulate (Fig. 3b). This is analogous to the case of Fe_3O_4 nanoneedles nucleating on the plated Fe nanocrystals, rather than from their gaps, during thermal oxidation [23]. In any case, the tapered W-ZnO whiskers extending along mosaic $\{10\bar{1}1\}$ and $\{2\bar{1}\bar{1}1\}$ surfaces, and twin boundaries can be more reasonably explained by precedent nanocondensates with such characteristics as mentioned.

Twinning Energetics and Mass Transport for the Tapered W-ZnO Whisker

The atomic structure and electronic effects of the $(11\bar{2}2)$ twin boundary in ZnO has been studied experimentally and theoretically using first-principle density-functional total-energy calculations [8]. The twin boundary was found to have the head-to-tail polarity configuration, which avoids dangling bonds, leading to a low twin-boundary energy of 0.040 J/m^2. The authors, investigations [8] of the electronic structure further revealed that the twin boundary does not introduce localized energy states in the band gap in W-ZnO. Such detailed electronic structure and atomic bonding at twin boundaries are out of the scope of this study. Instead, the crystallographic and energetic aspects for the growth of the present W-ZnO whisker with $(2\bar{1}\bar{1}1)$ vs $(1\bar{1}0\bar{1})$-specific twinning can be rationalized by their difference of lattice misfit [5]. It was pointed out that the $\{10\bar{1}1\}$ or $\{11\bar{2}1\}$ contact plane is allowed for coalescence twinning of W-ZnO crystallites involving rotation within 52.2 degree (cw or ccw) for both cases [5]. However, in comparison with $\{10\bar{1}1\}$, the $\{11\bar{2}1\}$ twin plane has much better coincidence on the lattice sites, in fact, with coincidence-site density of 1 in 6, i.e., $\Sigma = 6$ [5]. Thus $\{11\bar{2}1\}$ twin plane is an interfacial energy cusp for $\{hkil\}$-specific coalescence twinning [5] and beneficial for further extended growth to form the tapered whiskers with minor $\{10\bar{1}1\}$ twin boundaries nearly orthogonal to $\{11\bar{2}1\}$ twin plane as mentioned. The tapered ZnO whiskers in this study extend along mosaic twin domain boundaries rather than commonly observed [0001] direction. This can be rationalized by a rather rapid twinning growth kinetics taking advantage of the mass transport along the twin boundary [24].

The surface of a liquid alloy droplet was proved experimentally and theoretically to provide a favorable mass transport path for VLS growth [25]. The partially molten Zn particulate at the base of the tapered whisker would adopt such a rapid diffusion path. In addition, local whisker step/ledge with a curvature, as shown in Fig. 4e, could possibly involve the so-called surface premelting [26], despite a rather high bulk ZnO melting temperature of 1978 °C [27]. The initial smooth surface of nanocrystallites could become rough by surface premelting so that the atoms are not located on lattice positions and the layer has typical liquid-like short-range order [26]. However, it is less likely that surface premelting occurred along the well-developed $\{11\bar{2}1\}$ and $\{10\bar{1}1\}$ surface, in particular the latter having a significantly higher surface density than the former [5]. (The surface density of $\{11\bar{2}1\}$ and $\{10\bar{1}1\}$ are 6.47 and 10.04 atoms per nm^2, respectively, in terms of cation–anion-mixed and the outermost oxygen layer in the unrelaxed state [5].) In this connection, overheating experiment of lead particles [28] indicated that cubo-octahedra cannot, but {111} octahedral can be overheated (i.e., the close-packed {111} surfaces remained inert above the bulk Pb melting temperature. Temperature is also of concern to the growth rate anisotropy and surface energy, as shown by the formation of α-Fe_2O_3 nanobelts at ~700 °C whereas cylindrical nanowires at ~800 °C both forming mostly bicrystallites extending along [110], i.e., $[11\bar{2}0]$ direction during direct thermal oxidation of iron substrates under the flow of O_2 [29]. In any case, interdiffusion via the $\{11\bar{2}1\}$ and $\{10\bar{1}1\}$ surface or twin boundaries would be easier than lattice diffusion [30, 31] for the axial growth of whiskers. (The diffusivity of W-ZnO was reported to be 10^{-13}–10^{-15} cm^2/s for Zn^{2+} [30] and 10^{-15}–10^{-17} cm^2/s for O^{2-} [31] in the temperature range 900–1000 °C.)

It is noteworthy that the negatively charged Zn interstitials in coordination four and charge-compensating oxygen as well as Zn-on-O antisite are pertinent to n-type W-ZnO [32]. Future study is required to see how the oxygen partial pressure and system total pressure that played key roles in the growth of ZnO nanowires from various single crystal substrates [33] would affect the transport of such point defects and hence the growth of the tapered whiskers with mosaic twinning.

Implications

The formation of $\{10\bar{1}1\}/\{11\bar{2}1\}$-specific surface and mosaic twinning of the tapered W-ZnO whiskers by isothermal atmospheric annealing of the Zn particulates overlaid with W-ZnO condensates sheds light on an alternative VLS growth mechanism, i.e., {*hkil*}-specific coalescence twinning growth from the crystalline condensates taking advantage of a partially molten bottom source rather than a small liquid globular at the tip of the whisker. The ZnO whiskers when grown to a larger size and quantity can be removed by chemical and/or mechanical means from the Zn particulates for potential engineering applications. Further study is required to know whether such a mosaic twinning- and surface/interface diffusion-controlled VLS growth from bottom molten source, i.e., PLA-induced particulates, can be extended to the synthesis of other compound whiskers.

As for engineering applications, the present tapered W-ZnO whiskers in this syudy are promising seeds for growing larger crystals with unusual surface/twin boundaries. Such whiskers extending along polar $\{10\bar{1}1\}$ surfaces with mosaic $\{10\bar{1}1\}/\{11\bar{2}1\}$ twin boundaries yet with a strong photoluminescence at 391 nm and a considerable flexibility as shown in Fig. 8a and b, respectively, could have potential lasing/piezoelectric and energy-scavenging applications. The red shift of the near band edge emission in comparison with that of the sintered polycrystals (385 nm) (Fig. 8a), the [0001]-aligned rods (380 nm) [14], and taper-tubes (382 nm) [15] is possibly due to nanosize effect [34], the prevailed polar surfaces, and the mosaic-twinned domain boundaries of the present tapered whiskers in this study. Besides, a slight red shift and an increase in peak intensity were observed upon increasing the laser power. Such a phenomenon has been observed in thin ZnO films, which may indicate the presence of stimulated emission [35]. A novel nanostructure of nanobow in Fig. 8b is similar to that due to continuous and uniform bending of ZnO nanobelts [36]. In fact, bending of polar-surface-dominated nanobelt of ZnO can be attributed to electrostatic neutralization of the dipole moment via deformation (called an electrostatic polar charge model) and/or imbalances between surface tensions via surface-termination-induced stresses [36]. The bending modulus of such a ZnO ring has been experimentally determined as 109 GPa [37]. The self-organized, [0001] oriented W-ZnO nanowire arrays grown on suitable substrates can be used as room-temperature ultraviolet lasing materials [35]. The W-ZnO microfiber–nanowire hybrid structure was also demonstrated to be effective for energy scavenging from mechanical vibration/friction of the nanowires [38] taking advantage of the AC frequency-dependent piezoelectric coefficient (14.3–26.7 pm/V) [39] and the elastic bending dependence of conductance [37] for the [0001]-oriented W-ZnO nanowire with a rather high fracture strength of ca. 7 GPa [40]. Photoelectronic application, such as field emission, of the whiskers is also possible depending on other factors besides morphology. The tapered ZnO whiskers bounded by unusual crystal surfaces could have novel applications such as nanoforce/nanopressure sensors, nanocantilevers, field effect transistors and nanoresonants as shown for other (*hkil*)-specific ZnO nanobelts [41].

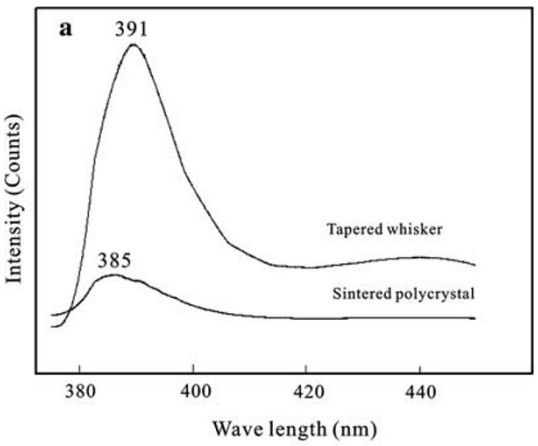

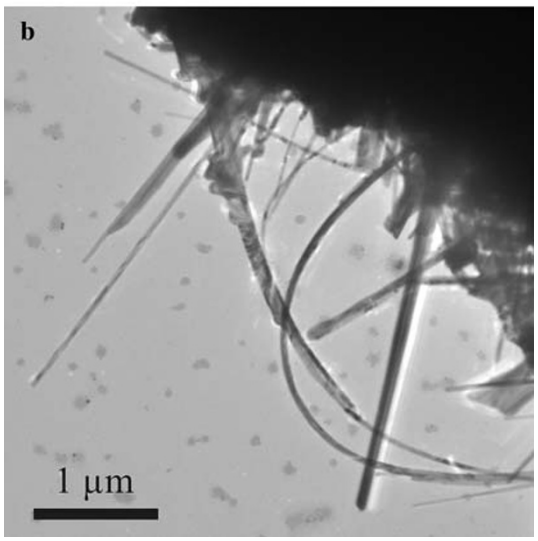

Fig. 8 **a** PL spectra of the tapered W-ZnO whisker showing strong luminescence at 391 nm with a significant red shift in comparison with the broad and weak signal at 385 nm for a polycrystalline W-ZnO standard; **b** TEM BFI showing that the tapered W-ZnO whisker is flexible to bend. The tapered whiskers are of the same specimen as in Fig. 3b

Conclusions

(1) Thermal oxidation of Zn particulates overlaid with W-ZnO condensates having $\{10\bar{1}1\}$ and $\{11\bar{2}1\}$ facets caused tapered W-ZnO whiskers with mosaic twinning.

(2) The tapered whisker slabs have $\{10\bar{1}1\}$- and $\{2\bar{1}\bar{1}1\}$-twinned domains due to $\{hkil\}$-specific coalescence and twinning growth along a common zone axis of the twin planes.

(3) The VLS growth of such twinned and tapered W-ZnO whiskers was facilitated by a partially molten bottom source of Zn and a sort of capillary diffusion of Zn atoms from the bottom to the tip of the whisker along the twinning edges and stepwise ledges as the source of tip growth.

Acknowledgments We thank C.N. Huang for his technical assistance on laser ablation, and L.J. Wang for her technical assistance on AEM, and anonymous referees for constructive comments. This research was supported by the Center for Nanoscience and Nanotechnology at NSYSU, and The National Science Council, Taiwan, ROC under contract NSC96-2221-E214-037 & NSC97-2221-E214-007.

Appendix

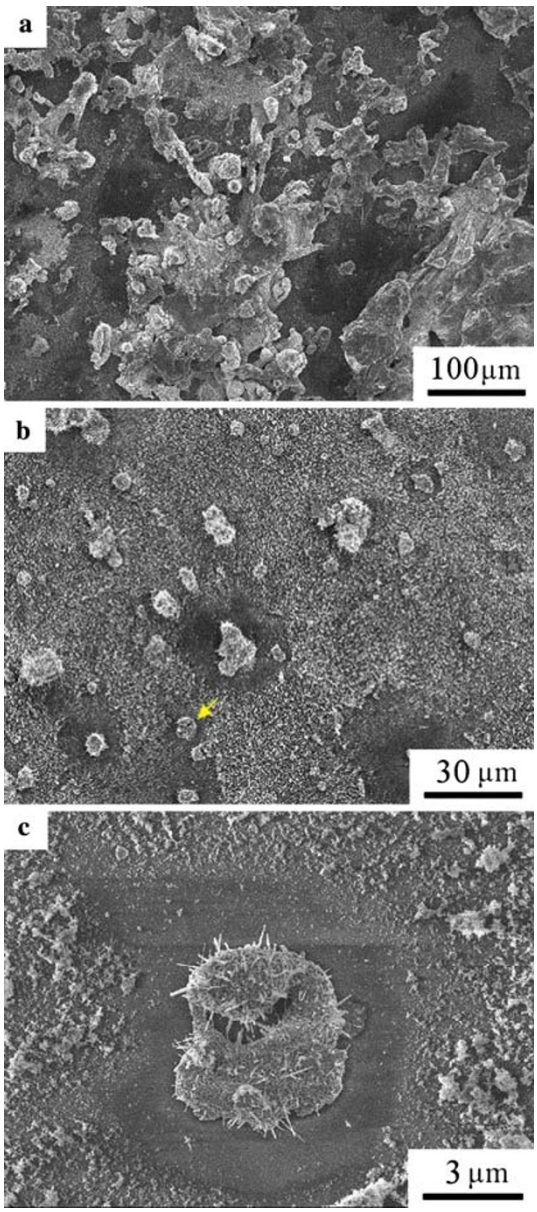

Auxiliary SEM secondary electron images of Zn/W-ZnO particulates subjected to post-deposition annealing: (**a**) As-deposited Zn molten plume with irregular shape; (**b**) further annealed at 600 °C for 1 h in air for the development of W-ZnO whiskers via a thermal oxidation VLS process from the globular particulates associated with the Zn-plume craters as indicated by the arrowed area magnified in (**c**)

References

1. R.S. Wagner, W.C. Ellis, Appl. Phys. Lett. **4**, 89 (1964). doi:10.1063/1.1753975
2. Z.W. Pan, Z.R. Dai, Z.L. Wang, Science **291**, 1947 (2001). doi:10.1126/science.1058120
3. Y. Ding, P.X. Gao, Z.L. Wang, J. Am. Chem. Soc. **126**, 2066 (2004). doi:10.1021/ja039354r
4. Z.L. Wang, X.Y. Kong, Y. Ding, P. Gao, W.L. Hughes, R. Yang, Y. Zhang, Adv. Funct. Mater. **14**, 943 (2004). doi:10.1002/adfm.200400180
5. B.H. Huang, S.Y. Chen, P. Shen, J. Phys. Chem. C **112**, 1064 (2008). doi:10.1021/jp076601v
6. Y. Gui, C. Xie, Appl. Phys. (Berl) **15**, 164 (1944)
7. Q.F. Lu, H.X. Wei, Z.D. Hu, Am. Mineral. **50**, 22 (1965)
8. Y. Yan, M.M. Al-Jassim, M.F. Chisholm, L.A. Boatner, S.J. Pennycook, M. Oxley, Phys. Rev. B **71**, 041309 (2005). doi:10.1103/PhysRevB.71.041309
9. Y. Dai, Y. Zhang, Y.Q. Bai, Z.L. Wang, Chem. Phys. Lett. **375**, 96 (2003). doi:10.1016/S0009-2614(03)00823-6
10. Y. Ding, Z.L. Wang, T. Sun, J. Qiu, Appl. Phys. Lett. **90**, 153510–153511 (2007). doi:10.1063/1.2722671
11. Y. Gui, C. Xie, Mater. Chem. Phys. **93**, 539 (2005). doi:10.1016/j.matchemphys.2005.04.006
12. Q.F. Lu, H.X. Wei, Z.D. Hu, Trans. Nonferrous Metab. Soc. China **14**, 973 (2004)
13. X. Wu, H. Bai, C. Li, G. Lu, G. Shi, Chem. Commun. Camb. **15**, 1655 (2006). doi:10.1039/b516497d
14. C. Yan, D. Xue, J. Cryst. Growth **310**, 1836 (2008). doi:10.1016/j.jcrysgro.2007.10.060
15. C. Yan, D. Xue, Electrochem. Commun. **9**, 1247 (2007). doi:10.1016/j.elecom.2007.01.029
16. C. Yan, J. Liu, F. Liu, J. Wu, K. Gao, D. Xue, Nanoscale Res. Lett. **3**, 473 (2008). doi:10.1007/s11671-008-9193-6
17. C. Yan, D. Xue, J. Phys. Chem. B **110**, 25850 (2006). doi:10.1021/jp0659296
18. D.B. Chrisey, G.K. Hubler, *Pulsed Laser Deposition of Thin Films* (Wiley, New York, 1994)
19. D. Stull, in *American Institute of Physics Handbook*, 3rd edn, ed. by D.E. Gray (McGraw Hill, New York, 1972)
20. D.B. Williams, *Practical analytical electron microscopy in materials science* (Philips Electronic Instruments Inc, Mahwah, 1984)
21. G.P. Panasyuk, M.N. Danchevskaya, N.I. Kobozev, Zh.Fiz. Khim **41**, 691 (1967). (in Russian); Diffusion Data **1**, R66
22. R. Wu, C. Xie, J. Hu, H. Xia, A. Wang, Scr. Mater. **43**, 841 (2000). doi:10.1016/S1359-6462(00)00500-5
23. Y. Liu, L. Liao, C. Pan, J. Li, Y. Dai, W. Chen, J. Phy, Chem. Can. **112**, 902 (2008)
24. D.A. Porter, K.E. Easterling, *Phase Transformations in Metals and Alloys* (CRC Press, USA, 1992)
25. H. Wang, G.S. Fischman, J. Appl. Phys. **76**, 1557 (1994). doi:10.1063/1.358515
26. J.J. Métois, J.C. Heyraud, Ultramicroscopy **31**, 73 (1989). doi:10.1016/0304-3991(89)90036-3
27. D.D. Wagman, T.L. Jobe, E.S. Domalski, R.H. Schumn, in *American Institute of Physics Handbook*, 3rd edn, ed. by D.E. Gray (McGraw Hill, New York, 1972)
28. J.J. Métois, J.C. Heyraud, J. Phys. **50**, 3175 (1989)
29. X. Wen, S. Wang, Y. Ding, Z.L. Wang, S. Yang, J. Phys. Chem. B **109**, 215 (2005). doi:10.1021/jp0461448
30. G.W. Tomlins, J.L. Routbort, T.O. Mason, J. Appl. Phys. **87**, 117 (2000). doi:10.1063/1.371832
31. A.C.S. Sabioni, M.J.F. Ramos, W.B. Ferraz, Mater. Res. **6**, 173 (2003)
32. Ü. Özgür, Y.I. Alivov, C. Liu, A. Teke, M.A. Reshchikov, S. Doğan, V. Avrutin, S.J. Cho, H. Morkoç, J. Appl. Phys. **98**, 041301 (2005). doi:10.1063/1.1992666
33. X. Wang, J. Song, Z.L. Wang, J. Mater. Chem. **17**, 711 (2007). doi:10.1039/b616963p
34. Y. Gong, T. Andelman, G.F. Neumark, S. O'brien, I.L. Kuskovsky, Nanoscale Res. Lett. **2**, 297 (2007). doi:10.1007/s11671-007-9064-6
35. M.H. Huang, Y. Wu, H. Feick, N. Tran, E. Weber, P.D. Yang, Adv. Mater. **13**, 113 (2001). doi:10.1002/1521-4095(200101)13:2<113::AID-ADMA113>3.0.CO;2-H
36. W. Hughes, Z.L. Wang, J. Am. Chem. Soc. **126**, 6703 (2004). doi:10.1021/ja049266m
37. X. Wang, J. Zhou, J. Song, J. Liu, N. Xu, Z.L. Wang, Nano Lett. **6**, 2768 (2006). doi:10.1021/nl061802g
38. Y. Qin, X. Wang, Z.L. Wang, Nature **451**, 809 (2008). doi:10.1038/nature06601
39. M.H. Zhao, Z.L. Wang, S.X. Mao, Nano Lett. **4**, 587 (2004). doi:10.1021/nl035198a
40. C.Q. Chen, J. Zhu, Appl. Phys. Lett. **90**, 043105 (2007). doi:10.1063/1.2432289
41. Z.L. Wang, J. Phys. Cond. Mater. **16**, R829 (2004). doi:10.1088/0953-8984/16/25/R01